Lattice model results for lamellar phases in slits

M. Tasinkevych and A. Ciach
Institute of Physical Chemistry and College of Science, Polish Academy of Sciences, Kasprzaka 44/52, 01-224 Warsaw, Poland
(Received 5 May 1999)

A mixture of oil, water, and surfactant confined between parallel hydrophilic walls is studied close to phase boundaries between lamellar and uniform phases within a vector lattice model in a mean-field approximation. Relations between energy and force-distance profiles, and the structure of the confined fluid (given by density profiles) are found and discussed. For large wall separations L elastic response to compression or decompression, accompanied by shrinking or swelling of the period λ of the lamellar phase, is found for lamellar and induced (by capillary condensation) lamellar phases. Very good agreement with recent experiments is obtained. For $L<4\lambda$ the system responds to decompression by swelling of the central, either oil- or water-rich layer, with the layers adsorbed at the surfaces remaining unaffected. The solvation force is very weak and independent of L when the central layer is swollen, and jumps to much larger values when new layers are introduced into the slit. [S1063-651X(99)02212-6]

PACS number(s): 68.15.+e, 68.55.−a, 68.60.−p

I. INTRODUCTION

Confinement has a significant effect on fluids, particularly near continuous or first-order phase transitions [1,2]. In order to keep the confining walls at a given distance L, an external force must be applied. For fluids confined between two parallel walls this force, per unit area of a confining wall, is called solvation force or disjoining presure [3], f, and can be expessed as an excess pressure over the bulk value p [1]:

$$f=-\frac{1}{A}\left(\frac{\partial\Omega}{\partial L}\right)_{\mu,T,A}-p, \tag{1}$$

Ω is the grand-thermodynamic potential and A is the surface area of one wall ($A\gg L^2$). For simple fluids the solvation force measured in surface force apparatus experiments [4] shows oscillatory behavior for separations up to several diameters of fluid particles [5], and with the periodicity approximately equal to one fluid molecular diameter. Oscillatory f results from the packing effects, which also give rise to highly structured density profile $\rho(z)$. All structural deformations and/or transitions occurring in confined systems (capillary condensation, layering) are reflected in the behavior of the solvation force. Hence the surface force apparatus measurements provide experimental information about the structure and transitions in the confined systems.

Close to the phase transitions the characteristic lengths such as a range of correlations or a thickness of a wetting layer become large. As the finite-size effects occur when L is comparable to the lengths characteristic for the fluid, close to the phase transitions one expects finite-size effects for L up to hundreds of Å. In the case of self-assembling systems, such as copolymers, binary, or ternary surfactant mixtures, lipids, etc., additional lengths, corresponding to the typical size of the nanostructure, are present. In microemulsions the typical lengths are the size of oil- or water-rich domains λ, and the distance over which the domains are correlated. In lamellar phases the typical length λ is the period of oscillations of the concentrations of all the components. Whereas in the case of simple fluids the finite-size effects are relevant for small systems (far from phase transitions up to ~ 10 molecular diameters) in the case of complex fluids $\lambda\sim 10$ nm, but can be as large as 100 nm and the finite-size effects can be relevant for $L\sim 100-1000$ nm.

Confined lamellar phases have been extensively studied by surface force apparatus (SFA) measurements [6–11]. The homeotropic alignment of the lamellar phase was obtained between SFA surfaces [9], which therefore impose a strain on the whole stack of lamellae. The measured force-distance profile oscillates with a periodicity well correlated with the period of density modulations of the bulk lamellar phase. Hence the oil- and water-rich domains play on the nanoscale a role similar to particles on the microscale. However, there are important differences between the complex fluids on the nanoscale and simple fluids on the microscale, related, for example, to compressibility of the water and oil regions. The experiments show that for sufficiently large wall separations the confined stack of lamellae can be approximated by a chain of identical springs. Each spring corresponds to one period of the lamellar phase. When the wall separation is increased from the equilibrium positions by half of the period of the oscillations, the solvation force changes discontinuously from the attractive to the repulsive one. This discontinuity corresponds to transitions at which a new lamellar layer is introduced between the walls [6,9,11], and a stretched structure abruptly changes into a shrunk one. The oscillating solvation force was measured for very large L, up to the largest distance for which the measurements were performed, $L=2$ μm [9]. Moreover, confinement induces the sponge (or microemulsion) to lamellar phase transition close to the phase boundary [11–13]. This phenomenon is an analog of the capillary condensation of simple fluids in narrow pores [1,14,15].

To explain the behavior of the confined system on the phenomenological level one assumes that self-assembled surfactant bilayers or monolayers behave as elastic, undulating membranes [16]. In this approach the average distance between the membranes can be determined by either electrostatic forces or steric repulsions between the membranes, resulting from undulations [8]. The modulus of compressibility

$\overline{B}$ of the confined system was related to the average distance between the membranes p, and was found to be proportional to $(k_BT)^2$, T being the temperature and k_B the Boltzmann constant, and inversely proportional to the membrane rigidity κ [16]. The relation approximately consistent with electrostatically stabilized lamellar structure, or with the lamellar phase stabilized by undulations [8,9,17–19] has been found for different substances. Recent direct measurements show, however, that the experimental points for $\overline{B}(p)$ lie in the region between the theoretical curves corresponding to two values of κ, which differ by $\approx 100\%$ [9]. Moreover, the phenomenological description is approximately valid only for sufficiently large wall separations L, equal to several (at least five) periods of the lamellar structure. The measured solvation force deviates more and more from the predicted elastic behavior when L is decreased. For $L<4\lambda$ the description based on elastic, undulating membranes is certainly oversimplified.

The confined microemulsions and lamellar phases have been studied within the Landau-Ginzburg approach in Refs. [20–23]. Discontinuity of the solvation force related to an insertion of a pair of surfactant monolayers has been observed [22]. In the microemulsion the oscillating density profiles have been found close to the transition to the lamellar phase [21]. Hence the theory qualitatively correctly predicts the key features of the confined self-assembling systems. For small wall separations $L<4\lambda$ it was found in Monte Carlo simulations of the Landau-Ginzburg model [24] that a layer of a disordered fluid, resembling microemulsion, develops in the center of the system [23,25]. However, the relation between the structure and the measurable solvation force has not been studied in these works.

Although there exist microscopic (or quasimicroscopic) models of ternary surfactant mixtures, neither of them has been applied for studying the effects of confinement yet. In such an approach the only assumptions concern the nature and strength of interparticle interactions. The real interactions are very complicated. However, the characteristic bulk properties of balanced ternary surfactant mixtures are qualitatively correctly described by simple generic models, such as the Ciach-Høye-Stell (CHS) model [26], in which only crucial properties of amphiphilic interactions are taken into account. Even the simplest models cannot be solved exactly, and one often uses a mean-field (MF) approximation. In this approach the self-assembling of amphiphiles into mono- or bilayers, formation of lamellar phases, undulations of the monolayers leading to smeared average surfactant density profiles are all results, rather than assumptions, in contrast to the phenomenological approaches. The discreteness of the lattice models seems to be their disadvantage. However, in the case of swollen lamellar phases, with $\lambda>10a$, a being the lattice constant, the discreteness does not play a major role. On the other hand, the lattice constant a, identified with the size of amphiphilies, sets a natural physical length scale. For confined systems, particularly for small wall separations, for which the phenomenological description breaks down, the existence of a physical length scale is an important advantage of the model.

With the help of the lattice CHS model one can calculate the density profiles, the excess free energy and the solvation force, and determine the relation between them. The results can be compared with experiments and with the predictions of the phenomenological theories, by which numerous assumptions of the latter can be verified. In the case of small wall separations ($L<4\lambda$) there are no predictions for the relation between the structure of the confined system and the behavior of the solvation force. Such relation is important, since it enables one to draw conclusions about the structure from an experimentally measurable quantity. Moreover, within the CHS model one can study relations between the properties of the confined and the bulk systems. In particular, the effect of the bulk metastable phases on the structure and elastic properties of the confined system can be determined.

In this work we consider confined uniform and lamellar phases near their phase boundary within the CHS lattice model and address questions listed above. In the next section we briefly describe the model and the methods of calculations. In Sec. III we discuss the mean-field results for the lamellar and water-rich phases between the walls. Finally in Sec. IV we present a short summary.

II. MODEL

In the CHS lattice model the orientational degrees of freedom of the surfactant particles are explicitly taken into account. The surfactant particles are represented by unit vectors pointing in the direction of the polar head groups. In general, M orientations of amphiphiles, uniformly distributed over a unit sphere can be considered [27]. Every lattice site is occupied by either oil, water, or an amphiphile in an orientation $\hat{\omega}_m$, $m=1,\ldots,M$, there are thus $2+M$ microscopic states $\hat{\rho}_i(\mathbf{x})$ at every lattice site $\mathbf{x}$. $\hat{\rho}_i(\mathbf{x})=1(0)$ if the site $\mathbf{x}$ is (is not) occupied by the state i, where $i=1,2,\ldots,2+M$ denotes water, oil, and surfactant in different orientations, respectively. In the limit $M\to\infty$ the model becomes similar to the models studied in Refs. [28–30], in which orientations of amphiphiles change continuously. Interaction between an amphiphile at site $\mathbf{x}$ and ordinary molecule at site $\mathbf{x}'$ is proportional to a scalar product between the orientation of the amphiphile and the distance between the particles, $\mathbf{x}-\mathbf{x}'$, as in other lattice vector models [26,28,29,31–34] of surfactant mixtures.

In the simplest version of the CHS model the orientations are restricted to the $2d$ principal directions of the d-dimensional simple cubic lattice, i.e., $M=2d$, and surfactant particles in different orientations are treated as separate species. The states $i=1+2\alpha,2+2\alpha$ ($\alpha=1,\ldots,d$) correspond to a surfactant particle with the polar end pointing towards $-x_\alpha$th and $+x_\alpha$th directions, respectively. In the case of oil-water symmetry and in the close-packed system the only relevant chemical potential variable is the difference $\Delta\mu=\mu_1-\mu_3$, since $\mu_1=\mu_2$.

The Hamiltonian of the system confined between two identical surfaces $x_d=0$ and $x_d=L+1$, perpendicular to the d direction, can be written in the following form:

$$H=\frac{1}{2}\sum_{\mathbf{x}\neq\mathbf{x}'}\sum_{i,j}\hat{\rho}_i(\mathbf{x})\mathrm{U}_{ij}(\mathbf{x}-\mathbf{x}')\hat{\rho}_j(\mathbf{x}')+\sum_{\mathbf{x}}\sum_{i}h_i(\mathbf{x})\hat{\rho}_i(\mathbf{x})$$
$$-\Delta\mu\sum_{\mathbf{x}}[\hat{\rho}_1(\mathbf{x})+\hat{\rho}_2(\mathbf{x})]. \qquad (2)$$

Here the summations are taken only over the region $0<x_d<L+1$. $U_{ij}(\mathbf{x}-\mathbf{x}')$ is the interaction energy between particles of species i,j at the sites $\mathbf{x},\mathbf{x}'$ respectively, and $h_i(\mathbf{x})$ is the surface field acting on the particle i at the site $\mathbf{x}$. Here we choose for $U_{ij}(\mathbf{x}-\mathbf{x}')$ the form [35]:

$$\begin{aligned}U_{ij}(\mathbf{x}-\mathbf{x}')=\sum_{\alpha=1}^{d}\Big\{&-2b(\delta_{i1}\delta_{j1}+\delta_{i2}\delta_{j2})\delta(\mathbf{x}-\mathbf{x}'-\mathbf{e}_\alpha)\\&-2c(\delta_{i1}\delta_{j1+2\alpha}-\delta_{i1}\delta_{j2+2\alpha}-\delta_{i2}\delta_{j1+2\alpha}\\&+\delta_{i2}\delta_{j2+2\alpha})[\delta(\mathbf{x}-\mathbf{x}'+\mathbf{e}_\alpha)-\delta(\mathbf{x}-\mathbf{x}'-\mathbf{e}_\alpha)]\\&-g\sum_{\beta\neq\alpha}(\delta_{i1+2\alpha}\delta_{j1+2\alpha}+\delta_{i2+2\alpha}\delta_{j2+2\alpha}\\&-2\delta_{i1+2\alpha}\delta_{j2+2\alpha})[\delta(\mathbf{x}-\mathbf{x}'+\mathbf{e}_\beta)\\&+\delta(\mathbf{x}-\mathbf{x}'-\mathbf{e}_\beta)]\Big\}.\end{aligned}\tag{3}$$

$\mathbf{e}_\alpha$ are the unit vectors of the lattice and δ is the Kronecker symbol. All the coupling constants are chosen positive; b favors separation of oil from water, g favors formation of surfactant monolayers, and c describes amphiphilic interactions. In the simplest, symmetrical version of the model c is the attraction between the water and the polar end of the surfactant particles and also between the oil and the nonpolar end of the surfactant particles. At the same time c describes the repulsion between the water and the nonpolar end of the surfactant particles and also between the oil and the polar end of the surfactant particles. If we assume that the surfaces of the external walls are covered by water, then the surface field $h_i(\mathbf{x})$ is a function of x_d and can be written as

$$\begin{aligned}h_i(x_d)=&-b\delta_{i1}(\delta(x_d-1)+\delta(x_d-L))-c(\delta_{i1+2d}\\&-\delta_{i2+2d})\delta(x_d-1)-c(\delta_{i2+2d}-\delta_{i1+2d})\delta(x_d-L).\end{aligned}\tag{4}$$

Such a surface field favors formation of the lamellar film parallel to the surfaces.

Within the mean-field (MF) approximation the microscopic configurations $\hat{\rho}_i(\mathbf{x})$ occur with a probability proportional to the Boltzmann factor

$$\exp\Big[-\frac{1}{k_BT}\sum_{\mathbf{x}}\sum_{i}\Big\{\phi_i(\mathbf{x})\Big[\hat{\rho}_i(\mathbf{x})-\frac{1}{2}\rho_i(\mathbf{x})\Big]-[\mu_i+h_i(\mathbf{x})]\hat{\rho}_i(\mathbf{x})\Big\}\Big],\tag{5}$$

where $\phi_i(\mathbf{x})=\Sigma_{\mathbf{x}'}\Sigma_j U_{ij}(\mathbf{x}-\mathbf{x}')\rho_j(\mathbf{x}')$ is the mean field and $\rho_i(\mathbf{x})$ is the MF average of $\hat{\rho}_i(\mathbf{x})$. The grand-thermodynamic potential in MF takes the form

$$\Omega(\tau,\mu,L)=\sum_{\mathbf{x}}\sum_{i}\rho_i(\mathbf{x})\Big(\tau\ln[\rho_i(\mathbf{x})]+\frac{1}{2}\phi_i(\mathbf{x})+h_i(x_d)-\mu(\delta_{i1}+\delta_{i2})\Big),\tag{6}$$

where $\tau=k_BT/b$ is the temperature in the energy unit, $\mu=\Delta\mu/b$, and Ω is also measured in units of b. The distance in Eq. (6) is measured in units of the lattice constant, $a\sim 25$ Å, comparable to the size of amphiphiles.

The equilibrium densities $\rho_i(\mathbf{x})$ correspond to the global minimum of the thermodynamic potential Ω. In practice, however, we can only determine the densities corresponding to local minima of Ω by solving the set of the self-consistent equations:

$$\rho_i(\mathbf{x})=\frac{\exp\Big(-\frac{1}{\tau}[\phi_i(\mathbf{x})+h_i(x_d)-\mu(\delta_{i1}+\delta_{i2})]\Big)}{\sum_j\exp\Big(-\frac{1}{\tau}[\phi_j(\mathbf{x})+h_j(x_d)-\mu(\delta_{j1}+\delta_{j2})]\Big)}.\tag{7}$$

There are many local minima of Ω, corresponding to uniform phases and α-dimensional periodic structures. In the present work we restrict our attention to the lamellar phases. The lamellar phase confined between two parallel walls usually attains the homeotropic orientation, in which the lamellae are parallel to the walls. In this case the direction perpendicular to the walls is distinguished and the in-plane orientational degrees of freedom turn out to be irrelevant. Then $\rho_i(\mathbf{x})\mapsto\rho_i(z)$ and

$$\begin{aligned}\phi_i(\mathbf{x})\mapsto\phi_i(z)=&-2(d-1)\{b\delta_{i1}\rho_1(z)+b\delta_{i2}\rho_2(z)\\&+g(\delta_{i3}-\delta_{i4})[\rho_3(z)-\rho_4(z)]\}\\&+\sum_{z'=1}^{L}\sum_{j}U_{ij}(z-z')\rho_j(z'),\end{aligned}\tag{8}$$

where we simplified the notation by introducing $z\equiv x_d$, $\rho_3(z)\equiv\rho_{1+2d}(z)$, $\rho_4(z)\equiv\rho_{2+2d}(z)$. The first term in Eq. (8) is the in-plane energy contribution, and

$$\begin{aligned}U_{ij}(z-z')=&-2b(\delta_{i1}\delta_{j1}+\delta_{i2}\delta_{j2})\delta(z-z'+1)\\&-2c(\delta_{i1}\delta_{j3}-\delta_{i1}\delta_{j4}-\delta_{i2}\delta_{j3}\\&+\delta_{i2}\delta_{j4})[\delta(z-z'+1)-\delta(z-z'-1)]\end{aligned}\tag{9}$$

is the interaction energy of the $1d$ version of the CHS model used in Ref. [36]. For the lamellar phases the grand-thermodynamic potential takes the form

$$\Omega_l(\tau,\mu,L)=A\sum_{z=1}^{L}\sum_{i}\rho_i(z)\Big\{\tau\ln[\rho_i(z)]+\frac{1}{2}\phi_i(z)+h_i(z)-\mu(\delta_{i1}+\delta_{i2})\Big\},\tag{10}$$

with A being the area of the confining surface.

We solve Eq. (7) by means of numerical iterations starting from initial conditions of three types. The first two correspond to the uniform water-rich phase (in the case of hydrophilic surfaces) and to microemulsion. The third type consists of one-dimensional oscillations of different periods. We assume that the initial local densities are either 1 or 0.

To study the structural deformations of the system confined between surfaces of area A we calculate the excess quantity σ, given (in units of b) by

$$\sigma(\tau,\mu,L)=\frac{1}{A}\Omega_l(\tau,\mu,L)-L\omega_b(\tau,\mu). \tag{11}$$

The grand-thermodynamic potential of the bulk system per lattice site, ω_b, is calculated by using periodic boundary conditions in systems of various sizes, which correspond to one, two, or more periods of an infinite periodic structure. In this way we can obtain metastable structures with periods which are rational numbers. The lowest thermodynamic potential per lattice site corresponds to the stable phase and determines the period of the structure. σ is the effective interaction energy per unit area between the walls plus a term independent of L and related to the total wall-fluid interfacial tension. Then $-\partial\sigma/\partial L$ is the solvation force needed to held the walls at the separation L.

III. MEAN-FIELD RESULTS

A. $d=1$ case

The phase diagram of the one-dimensional system was calculated in Ref. [36]. It was found that for $c/b=1$ the swollen lamellar phase coexists with uniform water-/oil-rich phases (water-oil symmetry was assumed) at low surfactant concentration ($\rho_s\sim 0.12$). Because the discreteness of the model should not play an important role for the swollen lamellar phases ($\lambda\sim 10$), we first study the structural deformations of the confined swollen lamellar phases in the one-dimensional version of the CHS model.

1. Swollen lamellar phases

Swollen lamellar phases are stable close to the coexistence with the water-rich phase (in the case of hydrophilic surfaces). We choose the thermodynamic variables $(\tau,\mu)\equiv(k_BT/b,\Delta\mu/b)$ such that $\tau=0.84$ and $|\mu-\mu_{coex}|=0.003$; for this thermodynamic state the swollen lamellar phase with the period of densities oscillations $\lambda=13$ is stable.

The excess thermodynamic potential per unit area σ and the solvation force f are shown in Fig. 1. The behavior of σ and f, as well as the structure of the confined system are different for the short $L<19$ ($L<3/2\lambda$), the intermediate $19<L<54$ ($3/2\lambda<L<4\lambda$), and the large $L>54$ ($L>4\lambda$) wall separations. We discuss the three cases separately.

Short surface separations. For surface separations $L<6$ ($L<\lambda/2$) the water-rich phase with average water density 15–20 % higher than in the bulk lamellar phase is stable in the slit [see Fig. 2(a)]. For larger surface separations one observes enhancement of the surfactant density at the surfaces [see Fig. 2(b)]. The structure of the surface surfactant-rich films remains almost unaffected by further increase of the surface separation for $L<18$ ($L<3/2\lambda$). For the separations up to $L=18$ the oil-rich film is formed between the surfactant films adsorbed at the surfaces [see Fig. 2(c)] and the interaction energy between the surfaces corresponds to the first minimum of the σ [see Fig. 1(a)]. The shape of the energy agrees qualitatively with the measured repulsive hydration fluctuation and attractive van der Waals forces in water between surfaces coated by bilayers of the uncharged lipids [37]. Further increase of the surface separation leads to formation of the first lamellar layer [see Fig. 2(d)].

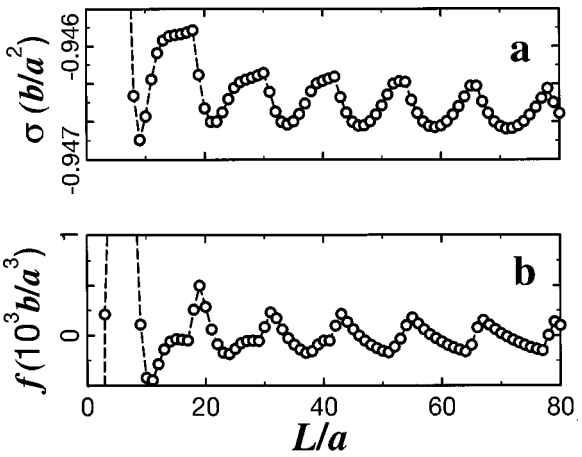

FIG. 1. (a) Excess thermodynamic potential σ [in units of b/a^2, b is the strength of the water-water (oil-oil) interaction], Eq. (11), as a function of the wall separation measured in units of the lattice constant a. (b) Solvation force f (in units of b/a^3) as a function of the wall separation. The thermodynamic variables τ, μ and the material constant c of the one-dimensional system correspond to stability of the swollen lamellar phase with $\lambda=13a$ ($\tau=0.84,\mu=0.774,c/b=1$); the distance from the first-order transition between the water-rich and the lamellar phases is $|\mu-\mu_{coex}|=0.003$. Walls are covered by water. Dashed lines are to guide the eye.

Intermediate surface separations. For the surface separations $19<L<54$ ($3/2\lambda<L<4\lambda$), for which the number of adsorbed layers is $N\leqslant 3$, the stretch strain of layers releases by formation of the uniform water-rich film for $N=1,3$ [see

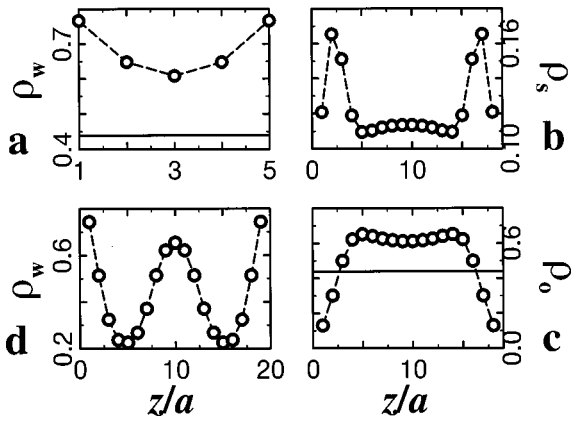

FIG. 2. One-dimensional system in the case of small wall separations measured in units of the lattice constant a, $L<19$. (a) The density distribution of water for the separation $L=5$. The solid line is the average water density in the bulk lamellar phase for the same values of τ,μ,c. (b) The density distribution of the surfactant, $\rho_s=\rho_3+\rho_4$ for the separation $L=18$. Note the surfactant-rich surface films. (c) The density distribution of oil for $L=18$. the solid line is the oil density in the bulk lamellar phase for the same conditions. (d) The density of the water for the wall separation $L=19$. The thermodynamic variables τ, μ and the material constant c are the same as in Fig. 1. Walls are covered by water. Dashed lines are to guide the eye.

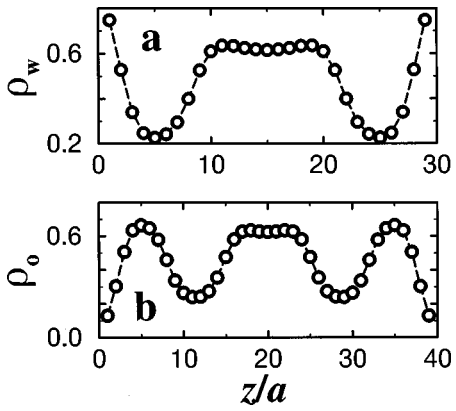

FIG. 3. One-dimensional system in the case of intermediate wall separations, $18<L<54$. The thermodynamic variables τ, μ and the material constant c are the same as in Fig. 1. Walls are covered by water. (a) The density distribution of water between walls for the separation $L=29$. (b) The density distribution of oil between walls for the separation $L=39$.

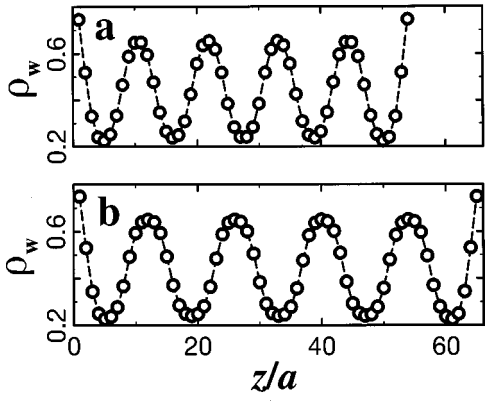

FIG. 4. One-dimensional system in the case of large wall separations, $L>53$. (a) the density distribution of water between the walls for the separation $L=54$. The period of the density oscillations is 11. (b) The density distribution of water for the wall separation $L=65$. The lamellar phase is stretched with the period of the oscillations equal to 13.75. The thermodynamic variables τ, μ and the material constant c are the same as in Fig. 1. Walls are covered by water.

Fig. 3(a)], and oil-rich film for $N=2$ [see Fig. 3(b)] in the middle of the slit. Similar phenomena were observed in simulations of the confined Landau-Ginzburg model with a single order parameter [23,25]. The formation of the uniform films inside the slit is reflected in the saturatedlike behavior of σ and considerably low f for the corresponding surface separations, see L around 52,40,27 in Fig. 1. For small deviations from the equilibrium separations the elastic behavior of the confined lamellar phase can be observed, see $L \approx 21,34,46$ in Fig. 1.

Large surface separations. For large separations between surfaces, $L>53$ $(L>4\lambda)$, the lamellar phase with the number of layers $N\geqslant 4$ is formed. The abrupt changes of the interaction energy per unit area σ and the solvation force f when the distance between the surfaces increases, correspond to the insertion of a new lamellar layer between the surfaces, that is N is increased by 1. Between two subsequent transitions σ has a minimum at $L=L_N$, which corresponds to the equilibrium surface separation and vanishing solvation force f. For such separations the structure of the confined fluid is equivalent to the structure of the bulk phase, namely, it has the same period of the densities oscillations. Decreasing or increasing the wall separation with respect to $L=L_N$, such that the number of adsorbed layers N stays constant ($L_N-\lambda/2<L<L_N+\lambda/2$), leads to the repulsive, $f>0$, or attractive, $f<0$ force between the surfaces, respectively. $f>0$ corresponds to the shrunk lamellar structures stabilized by confining surfaces; the period of densities oscillations λ is smaller than in the bulk phase, see Fig. 4(a). On the other hand, $f<0$ appears as a consequence of stretched lamellar structures, see Fig. 4(b), with the period of oscillations greater than in the bulk.

The subsequent energy minima of σ are well approximated by parabolic curves, even for quite large deviations from $L=L_N$. The second derivative of σ with respect to L calculated at $L=L_N$, $B=\sigma''(L_N)$, is well approximated by a straight line as a function of $1/N$ [see Fig. 5(a)]. Hence the response of the system to compression or decompression is elastic, and analogous to the behavior of a series of identical joined springs. The elastic constant $\overline{B}$ is related to B by $\overline{B}=2L_NB$, where B is calculated at L_N and L_N is the thickness of the system at zero stress [9]. We obtain $\overline{B}=0.003(k_BT/a^3)$. This finding is in accordance with the experimental results of Refs. [9,12]. The compressibility modulus measured in Ref. [9] for different volume fractions of surfactant ranges from 0.003 to 0.027, when expressed in units of k_BT/ϵ^3 (ϵ is the thickness of the membrane and is equal to 1.9 nm for the system studied in Ref. [9]). For large wall separations, $L>4\lambda$, our description gives thus results consistent with experiments, both for the qualitative bahavior as well as for the range of order of the measurable quantities.

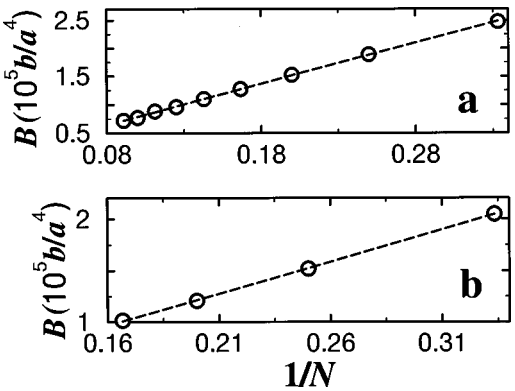

FIG. 5. The subsequent minima of σ are fitted by quadratic curves, $B(L-L_N)^2$, where L_N is the equilibrium separation for N adsorbed layers and B is the coefficient in the fitting curve to the Nth minimum. (a) B [in units of b/a^4, b is the strength of the water-water (oil-oil) interaction and a is the lattice constant] as a function of the inverse number of adsorbed layers $1/N$. The thermodynamic variables τ, μ and the material constant c are the same as in Fig. 1. (b) B (in units of b/a^4) obtained for the induced lamellar phases as a function of the inverse number of adsorbed layers $1/N$. The parameters τ, μ, and c correspond to the stability of the water-rich phase ($\tau=0.84,\mu=0.778,c/b=1$). The distance from the first-order transition to the swollen lamellar phase is $|\mu-\mu_{coex}|=0.001$. Dashed lines are linear fits.

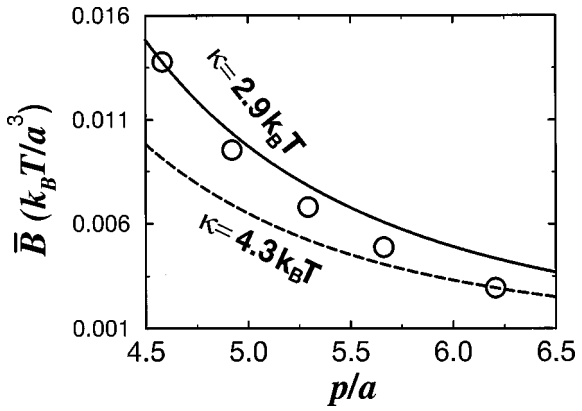

FIG. 6. Compressibility modulus $\bar{B}$ (in units of k_BT/a^3), of the swollen lamellar phases as a function of the average distance between the surfactant monolayers, $p=\lambda/2$, in the one-dimensional system. The behavior expected from the phenomenological description Eq. (12) is shown for two values of κ: $2.9k_BT$ (solid line), $4.3k_BT$ (dashed line).

In our approach $\bar{B}$ is calculated within the MF approximation for a quasimicroscopic lattice model, with no further assumptions concerning, for example, self-assembling of the surfactants, elastic properties and types of deformations of surfactant layers. The deformations of the equilibrium state occur in our theory with a probability given by Eq. (5). As the surfactant density profiles are smeared (see Fig. 4), the probabilities of the displacements of the surfactant monolayers from their equilibrium positions appear to be quite large. The displacements may correspond, among others, to the undulations considered in the phenomenological approach. We can verify whether $\bar{B}$ and λ calculated in our theory satisfy the relation obtained for a stack of confined elastic membranes in Refs. [16,17,38] which reads

$$\bar{B}=\frac{9\pi^2(k_BT)^2p}{64\kappa(p-\epsilon)^4}, \tag{12}$$

where $p=\lambda/2$ is the reticular spacing, ϵ is the membrane thickness which in our case equals 1, and κ is the membrane bending rigidity.

$\bar{B}$ as a function of p is shown in Fig. 6 (open circles). Our results lie between two lines correponding to $\bar{B}$ calculated according to formula (12) for $\kappa=2.9k_BT$ and $\kappa=4.3k_BT$. Experimental results for sodium bis(2-ethylhexyl) sulfosuccinate and brine, at $T=25°$ C lie between the lines given by Eq. (12) for $\kappa=0.5k_BT$ and $\kappa=3k_BT$ [9]. In the experimental system the thickess of the surfactant layer is 1.9 nm ($a\approx1.9$ nm). In our dimensionless units the reticular spacing in experimental and model systems are similar (see Fig. 6 here and Fig. 8 of Ref. [9]). The agreement is quite good—please note that we consider MF approximation for the one-dimensional version of the lattice model. Different substances in our model are characterized by different values of the interaction parameter c. The elastic properties depend on c and for different substances different values will be obtained. It is remarkable that the orders of magnitude of the elastic constants in the confined model and experimantal systems are the same if the periods of the bulk lamellar structure in our dimensionless units in the model and experimental systems are the same.

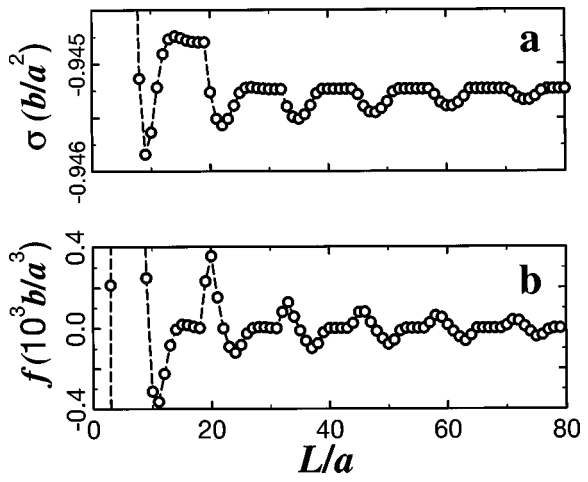

FIG. 7. (a) The excess thermodynamic potential σ [in units of b/a^2, b is the strength of the water-water (oil-oil) interaction] as a function of the wall separation measured in unit of the lattice constant a. (b) The solvation force f (in units of b/a^3) as a function of the wall separation. The thermodynamic variables τ, μ and the material constant c of the one-dimensional system correspond to the stability of the water-rich phase, close to the coexistence with the swollen lamellar phase ($\tau=0.84,\mu=0.778,c/b=1$, $|\mu-\mu_{coex}|=0.001$). Walls are covered by water.

Both experiments and our calculations show that the phenomenological theory is valid only approximately and there are substantial deviations from its predictions. It means that the membrane undulations are the most relevant deformations of the ideal lamellar structure, but the contributions from different deformations are not negligible.

2. Water-rich phase

Here we study the effect of confinement on the uniform solution. We choose the thermodynamic variables close to the coexistence with a swollen lamellar phase, $|\mu-\mu_{coex}|=0.001$. σ and f calculated as functions of the wall separa-

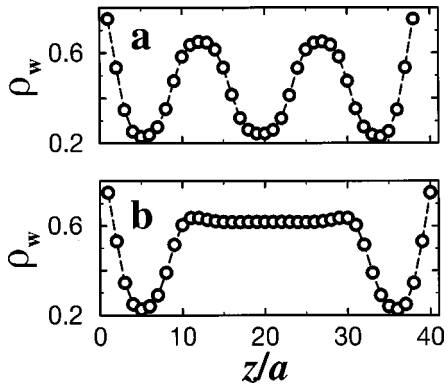

FIG. 8. (a) Density distribution of water between walls for the separation $L=38$ (the third minimum in the Fig. 7). (b) Density distribution of water between walls for the separation $L=40$. For such density distributions the solvation force vanishes. The parameters are the same as in Fig. 6 ($\tau=0.84,\mu=0.778,c/b=1$, $|\mu-\mu_{coex}|=0.001$).

tion are shown in Fig. 7. For small surface separations the sequence of structures formed inside the slit is similar to that obtained in the lamellar phases; the water-rich phase is stable for $L<6$, then surfactant layers are adsorbed at the surfaces for $L=6$ and the oil-rich phase stabilizes between the layers up to the separation $L=19$. The subsequent minima of σ correspond to the transitions when the lamellar phase with increasing number of layers is formed between the surfaces, see Fig. 8(a). The values of the surface separations for which the solvation force is zero correspond to the structures shown in Fig. 8(b), when the water-rich phase is formed inside the slit. The induced lamellar phases also show the elastic response to the confinement. In contrast to the case of the lamellar phases, the elastic response occurs only for small deviations from equilibrium separations, see Fig. 5(b). The elastic constant $\overline{B}$ is $\overline{B}\approx 0.002 k_B T/a^3$, and the membrane rigidity κ calculated according to Eq. (12) is $\sim 3.67 k_B T$. Again, we obtain the same orders of magnitude as in experiments [12].

In all the considered cases the equilibrium bulk densities were identified with the self-consistent solutions of the bulk analog of the set of Eq. (7) ($h_i=0$, periodic boundary conditions) giving the lowest value of the bulk grand-thermodynamic potential per lattice site. However, various local minima of the bulk thermodynamic potential also satisfy the same set of equations and correspond to metastable states. When the swollen lamellar phase with period 13 is stable in the bulk, the values of the thermodynamic potential of the metastable phases with somewhat smaller or larger periods or of the water-rich phase are only slightly greater (relative difference $\sim 10^{-5}$) from the equilibrium value. The same is true when the water-rich phase is stable in the bulk. Therefore the bulk metastable phases whose periods are commensurate with the surface separations become stable in the slit in our model. In the case of L and λ incommensurate with each other the increase of Ω corresponding to deformations of the structure is larger than the difference between Ω corresponding to the stable and the metastable phases, if the period of the latter is commensurate with L.

3. Shrunk lamellar phase

In the system with $c=4$ the bulk lamellar phase was found to be shrunk. The period of densities oscillations is always equal to 4. Close to the coexistence between the lamellar and the microemulsion phases only one metastable phase occurs apart from the other, stable one. This gives qualitatively different energy σ and solvation force f profiles.

The total wall-liquid interfacial tension σ and its part independent of L were calculated in Ref. [39]. Here we calculate the linear excess thermodynamic potential $\Delta(L)$ as a difference between the two quantities. $\Delta(L)$ calculated in the region of stability of the shrunk lamellar phase, close to the coexistence with the microemulsion, is shown in Fig. 9. The minima of $\Delta(L)$ occur for surface separations L_N commensurate with the period of densities oscillations $\lambda=4$ and correspond to N lamellar layers adsorbed in the slit. For the intermediate separations the adsorbed phases are deformed and the deformations are located at the midplane of the slit. For the separations up to $L=22$ the microemulsion films are formed in the middle of the slit, see Fig. 10(a), while for

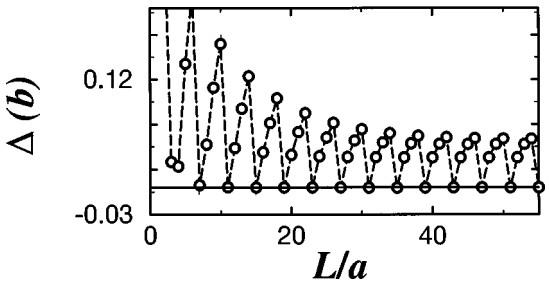

FIG. 9. Linear excess thermodynamic potential Δ (in units of b) as a function of the wall separation in the one-dimensional case. The thermodynamic variables τ, μ and the material constant c correspond to stability of the shrunk lamellar phase with the period of density oscillations equal to $4a$ ($\tau=2.8, \mu=4.32, c/b=4$). Solid line corresponds to vanishing Δ.

larger separations the strain releases to some extent by creating the lamellar films with suppressed amplitude, see Fig. 10(b). The discreteness of the model does not allow for further release of applied strain and as a consequence $\Delta(L)$ does not approach zero with increasing L. Please note that in experiments of Ref. [9] the oscillating solvation force was observed for all the measured distances, up to $L=1000$ in our dimensionless units.

B. $d=3$ case

σ calculated for $d=3$ and the thermodynamic variables τ, μ and the material constants c, g corresponding to the stability of the swollen lamellar phase with the period equal to 12 is shown in Fig. 11(a). All the structural deformations of the lamellar phase present in the one-dimensional system also hold in three dimensions, and no other deformations occur. For surface separations $L<5$ ($L<\lambda/2$) the water-rich films are induced by confinement, Fig. 12(a). The surfactant-rich surface films of thickness 4 [see Fig. 12(b)] occur first for the separation $L=5$ and are separated by the oil-rich phase for the separations up to $L=14$ [see Fig. 12(c)]. The first lamellar layer develops for the separation $L=15$ (slightly larger than λ) as shown in Fig. 12(d).

For the intermediate surface separations, $15<L<51$ (when the number of layers is $N\leqslant 3$), the system releases the stretch strain by forming the uniform film at the midplane of

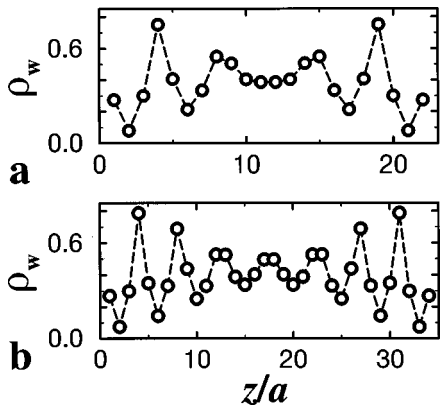

FIG. 10. Density profiles of water between water-covered walls for parameters $\tau=2.8$, $\mu=4.32$, $c=4$ (in units of b) (a) $L=22$ and (b) $L=34$.

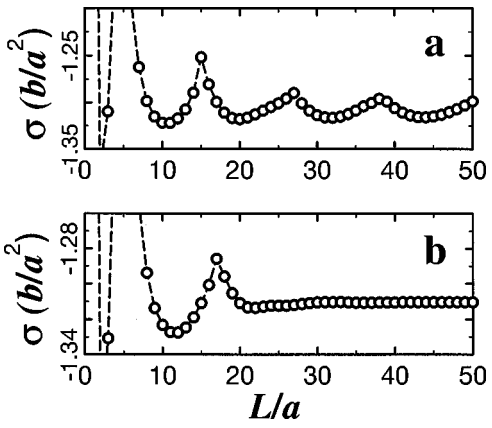

FIG. 11. The excess thermodynamic potential σ [in units of b/a^2, b is the strength of the water-water (oil-oil) interaction] as a function of the wall separation in the three-dimensional case with water-covered walls. (a) The thermodynamic variables τ, μ and the material constants c,g correspond to the stability of the swollen lamellar phase with the period equal to 12 lattice constant ($\tau=2.8,\mu=4.76,c/b=2.5,g/b=0.5$). (b) The parameters correspond to the stability of the water-rich phase ($\tau=2.8,\mu=4.82,c/b=2.5,g/b=0.5$).

the slit. This effect is less pronounced than in the one-dimensional case. The system also shows the elastic response to compression when the period in the confined system is smaller than in the bulk [Fig. 13(a)] and decompression when the period is larger [Fig. 13(b)].

The elastic constant $\bar{B}$ as a function of $p=\lambda/2$ is shown in Fig. 14 (open circles) together with the phenomenological curves (12) for two values of κ, between which our results are located. We can compare our results with the experimental results for sodium bis(2-ethylhexyl) sulfosuccinate and brine at $T=25°$ C, as we already did for $d=1$. In our dimensionless units (length measured in units of the length of the amphiphile a, and $\bar{B}$ measured in units of k_BT/a^3) the periods of the lamellar phase are in the same range in the model and in the experimental systems, and the values of $\bar{B}$ and κ in the model and experiment agree very well (compare Fig. 14 here and Fig. 8 in Ref. [9]). Hence, once the model parameters are choosen such that the dimensionless period of the bulk lamellar phase is the same as in the experiment, the elastic properties of the confined model and experimental systems agree quantiatatively very well. Given the simplifications of the model interactions and the MF approximation, the agreement between the theory and the experiment is remarkable.

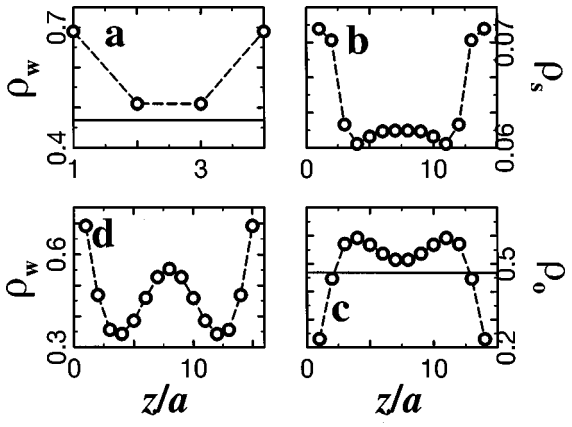

FIG. 12. The regime of small wall separations, $L<15$, in the 3D case. The values of τ, μ, c, and g correspond to the swollen bulk lamellar phase, as in Fig. 11(a). (a) The density distribution of water between walls for the separation $L=4$. Solid line corresponds to average water concentration in the bulk lamellar phase. (b) The density distribution of surfactant for the separation $L=14$. (c) The density distribution of oil for the wall separation $L=14$. Solid line is the oil concentration in the bulk lamellar phase. (d) The density of water for the separation $L=15$.

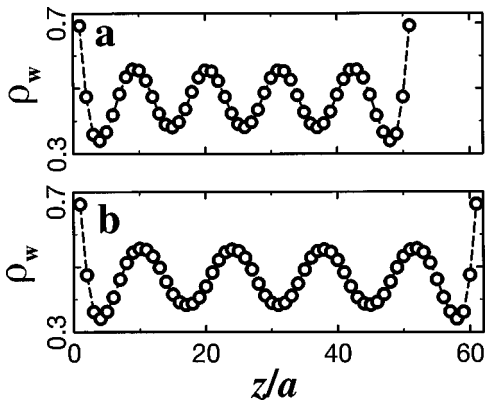

FIG. 13. The densities of water for large wall separation, $L>50$, are shown for (a) the wall separation $L=51$ and (b) the wall separation $L=61$. The values of parameters are the same as in Fig. 11(a) ($\tau=2.8,\mu=4.76,c/b=2.5,g/b=0.5$).

The energy-distance profile corresponding to the stability of the water-rich phase and close to the coexistence with the swollen lamellar phase is shown in Fig. 11(b). In the $3d$ system confinement induces only one lamellar layer, see Fig. 15(a), for appropriate wall separations, while for larger L the water-rich phase is formed in the middle of the slit, see Fig. 15(b).

IV. SUMMARY

In this work we applied the lattice CHS model of ternary surfactant mixtures for studying the effects of confinement.

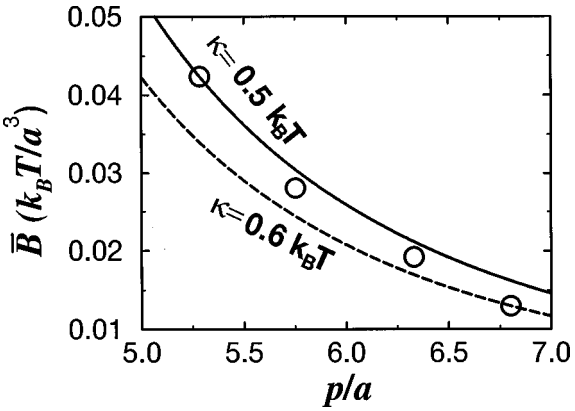

FIG. 14. Compressibility modulus $\bar{B}$ (in units of k_BT/a^3) of the swollen lamellar phases as a function of the average distance between surfactant monolayers, $p=\lambda/2$ (in units of a) in the three-dimensional system. The behavior expected from the phenomenological prediction is shown for two values of κ [Eq. (12)] $0.5k_BT$ (solid line), $0.6k_BT$ (dashed line).

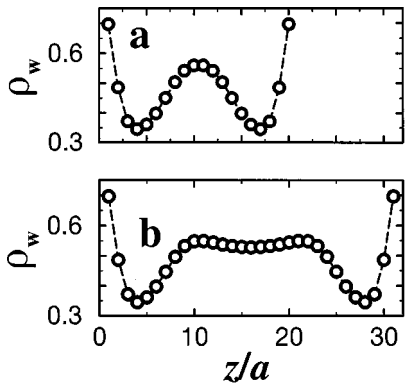

FIG. 15. (a) Density of water for the wall separation $L=20$ showing the ''capillary condensation'' of one lamellar layer. (b) Density of water for the wall separation $L=31$ showing that the water-rich film is formed inside the slit. The parameters correspond to stability of the water-rich phase as in Fig. 11(b) ($\tau=2.8, \mu=4.82, c/b=2.5, g/b=0.5$).

We concentrated on a slit geometry and hydrophilic walls and we calculated densities, excess grand-thermodynamical potential, and solvation force in lamellar and uniform phases within the MF approximation. In our approach the only assumptions concern the interparticle interactions and in MF the correlations between fluctuations are neglected. We consider a highly simplified model, in which a single dimensionless parameter, c/b, characterizes the strength of the amphiphilic interactions, that is, it specifies the system. No assumptions concerning the structure of the confined system are made.

For large wall separations we obtain results which are in a very good agreement with the results of recent experiments. We find elastic behavior of the confined lamellar phases, predicted also by membrane theories. The elastic response to compression or decompression is accompanied by shrinking or swelling of the period of the lamellar phase, whose structure is practically the same throghout the slit. Moreover, once the model parameters are choosen so that the period of the bulk lamellar phase (in units of the thickness of the surfactant monolayer) is in the same range as in the experimental system, then our results for elastic properties of the confined system agree quantitatively with experiments. The predictions of membrane theories agree only approximately with both our results and experiments. This suggests that in addition to undulations other configurations, such as passages between neighboring membranes are relevant. We get similar results for induced (''capillary condensation'') lamellar phases.

For intermediate and short wall separations $L<4\lambda$ we find the relation between the structure of the confined lamellar phase and the solvation force. When L is increased the central layer, either oil or water rich, swells, whereas surfactant-rich (or lamellar for $L>2\lambda$) layers adsorbed at the surfaces remain almost unchanged. The solvation force is very weak and almost independent of L when the central layer is swollen. When L becomes sufficiently close to being commensurate with λ, new surfactant monolayers are introduced into the slit and the solvation force jumps to a much larger value. This behavior is essentially different from the elastic behavior for $L>4\lambda$ accompanied by swelling or shrinking of the period of the lamellar phase. Now the system responds to compression or decompression by shrinking or swelling only the central, disordered layer, whereas the surfactant-rich (or lamellar for $L>2\lambda$) layers adsorbed at the surfaces remain almost unaffected. For some wall separations we find a swollen oil-rich layer in the middle of the slit. In such cases the density of oil in the slit is higher than in the bulk, despite the hydrophilic walls.

The results obtained in the one- and three-dimensional versions of the CHS model are qualitatively the same. The quantitative agreement with experiments in the $3d$ case is better.

ACKNOWLEDGMENT

This work was partially supported by KBN Grant No. 3T09A 073 16.

[1] P. Tarazona, U. M. B. Marconi, and R. Evans, Mol. Phys. **64**, 573 (1987).
[2] S. Dietrich, *Wetting Phenomena*, 1st ed., Phase Transitions and Critical Phenomena, Vol. 12 (Academic Press, London, 1988), pp. 1–218.
[3] B. V. Derjaguin, N. V. Churajev, and V. M. Müller, *Surface Forces* (Consultants Bureau, New York, 1987).
[4] J. N. Israelachvili and G. E. Adams, J. Chem. Soc., Faraday Trans. 1 **74**, 975 (1979).
[5] R. G. Horn and J. N. Israelachvili, J. Chem. Phys. **75**, 1400 (1981).
[6] P. Kékicheff and H. Christenson, Phys. Rev. Lett. **63**, 2823 (1989).
[7] P. Richetti, P. Kékicheff, J. L. Parker, and B. W. Ninham, Nature (London) **346**, 252 (1990).
[8] P. Kékicheff, P. Richetti, and H. Christenson, Langmuir **7**, 1874 (1991).
[9] D. A. Antelmi and P. Kékicheff, J. Phys. Chem. B **101**, 8169 (1997).
[10] O. Abillon and E. Perez, J. Phys. (Paris) **51**, 2543 (1990).
[11] P. Petrov, U. Olsson, H. Christenson, S. Miklavic, and H. Wennerström, Langmuir **10**, 988 (1994).
[12] P. Richetti, P. Kékicheff, and P. J. Barois, J. Phys. II **5**, 1129 (1995).
[13] P. Petrov, S. Miklavic, S. Olsson, and H. Wennerström, Langmuir **11**, 3928 (1995).
[14] B. K. Peterson, G. S. Heffelfinger, K. E. Gubbins, and F. van Swol, J. Phys. Chem. **93**, 679 (1990).
[15] R. Evans, J. Phys.: Condens. Matter **2**, 8989 (1990).
[16] W. Helfrich, Z. Naturforsch. A **33a**, 305 (1978).
[17] D. Roux and C. R. Safinya, J. Phys. (Paris) **49**, 307 (1988).
[18] F. Nallet, D. Roux, and J. Prost, Phys. Rev. Lett. **62**, 276 (1989).
[19] D. Roux, C. Coulon, and M. E. Cates, J. Phys. Chem. **96**, 4174 (1992).
[20] G. Gompper and S. Zschocke, Phys. Rev. A **46**, 4836 (1992).
[21] F. Schmid and M. Schick, Phys. Rev. E **48**, 1882 (1993).

[22] G. Gompper and M. Kraus, Phys. Rev. E **47**, 4289 (1993).
[23] R. Hołyst and P. Oswald, Phys. Rev. Lett. **79**, 1499 (1997).
[24] G. Gompper and M. Schick, Phys. Rev. Lett. **65**, 1116 (1990).
[25] R. Hołyst and P. Oswald, J. Chem. Phys. **109**, 11 051 (1998).
[26] A. Ciach, J. Høye and G. Stell, J. Phys. A **21**, L777 (1988).
[27] A. Ciach, J. Chem. Phys. **104**, 2376 (1996).
[28] G. Gompper and M. Schick, Chem. Phys. Lett. **163**, 475 (1989).
[29] J. R. Gunn and K. A. Dawson, J. Chem. Phys. **96**, 3152 (1992).
[30] M. W. Matsen, M. Schick, and D. E. Sullivan, J. Chem. Phys. **98**, 2341 (1993).
[31] M. W. Matsen and D. E. Sullivan, Phys. Rev. A **41**, 2021 (1990).
[32] M. Laradji, H. Guo, M. Grant, and M. J. Zuckermann, Phys. Rev. A **44**, 8184 (1991).
[33] P. A. Slotte, Phys. Rev. A **46**, 6469 (1992).
[34] M. W. Matsen and D. E. Sullivan, Phys. Rev. A **46**, 1985 (1992).
[35] A. Ciach and A. Poniewierski, J. Chem. Phys. **100**, 8315 (1994).
[36] A. Ciach, J. Chem. Phys. **93**, 5322 (1990).
[37] J. N. Israelachvili and P. M. McGuiggan, Science **241**, 795 (1988).
[38] S. Leibler and R. Lipowsky, Phys. Rev. B **35**, 7004 (1987).
[39] A. Ciach, M. Tasinkevych, and A. Maciołek, Europhys. Lett. **45**, 495 (1999).